# Coarse-grained models using local-density potentials optimized with the relative entropy: Application to implicit solvation

Tanmoy Sanyal, and M. Scott Shell

Citation: The Journal of Chemical Physics **145**, 034109 (2016); doi: 10.1063/1.4958629
View online: https://doi.org/10.1063/1.4958629
View Table of Contents: http://aip.scitation.org/toc/jcp/145/3
Published by the American Institute of Physics



# Coarse-grained models using local-density potentials optimized with the relative entropy: Application to implicit solvation

Tanmoy Sanyal and M. Scott Shell[a)]
*Department of Chemical Engineering, University of California Santa Barbara, Santa Barbara, California 93106, USA*

(Received 8 April 2016; accepted 21 June 2016; published online 20 July 2016)

Bottom-up multiscale techniques are frequently used to develop coarse-grained (CG) models for simulations at extended length and time scales but are often limited by a compromise between computational efficiency and accuracy. The conventional approach to CG nonbonded interactions uses *pair* potentials which, while computationally efficient, can neglect the inherently multibody contributions of the local environment of a site to its energy, due to degrees of freedom that were coarse-grained out. This effect often causes the CG potential to depend strongly on the overall system density, composition, or other properties, which limits its transferability to states other than the one at which it was parameterized. Here, we propose to incorporate multibody effects into CG potentials through additional nonbonded terms, beyond pair interactions, that depend in a mean-field manner on local densities of different atomic species. This approach is analogous to embedded atom and bond-order models that seek to capture multibody electronic effects in metallic systems. We show that the relative entropy coarse-graining framework offers a systematic route to parameterizing such local density potentials. We then characterize this approach in the development of implicit solvation strategies for interactions between model hydrophobes in an aqueous environment. *Published by AIP Publishing.* [http://dx.doi.org/10.1063/1.4958629]

## I. INTRODUCTION

Molecular dynamics (MD) simulations with detailed atomic resolution have advanced greatly over the last few decades due to hardware and algorithm improvements, particularly in terms of tractable system size.[1] However, coarse-grained (CG) models have become essential counterparts to all-atom (AA) modeling, bridging their limitations potentially in orders of magnitude further in length and time scales through the elimination of unnecessary details and identification of emergent physical models. In particular, "bottom-up" CG strategies seek to systematically remove degrees of freedom by grouping two or more atoms into a single CG "pseudoatom" or "site." While such methods have seen a flurry of activity in the past two decades,[2–12] a major outstanding challenge is achieving computationally efficient ways to represent CG interactions faithfully. In principle, by integrating out degrees of freedom in an AA model, the appropriate effective interaction "potential" between the remaining CG sites is a multidimensional potential of mean force (PMF), which is unique to an additive constant,[8,13–16]

$$W(\mathbf{R}) = -k_B T \ln \int_V d\mathbf{r} \exp\left[-\beta u(\mathbf{r})\right] \delta\left(\mathbf{R} - \mathbf{M}(\mathbf{r})\right). \quad (1)$$

Here, $V$ and $T$ are the system volume and temperature, respectively, $u(\mathbf{r})$ is the inter-atomic potential that is a function of the atomic positions $\mathbf{r}$, and the integral spans all values of $\mathbf{r}$ consistent with the system volume $V$. $\mathbf{M}(\mathbf{r})$ is a "mapping function" that translates an atomic configuration $\mathbf{r}$ to a CG one $\mathbf{R}$. For the special case in which the center of mass of a group of atoms is mapped onto a single CG site, $\mathbf{M}$ becomes a $n \times N$ matrix, where $n$ is the number of atoms in the AA system and $N$ is the number of CG sites. The Dirac delta function within the integral thus serves to project the AA potential energy surface along the reduced degrees of freedom ($\mathbf{R}$) of the CG model.

Bottom-up strategies seek CG forcefields that well-approximate $W$, but two challenges arise. First, $W$ is by nature a multibody interaction because CG degrees of freedom are highly coupled through the AA ones that were integrated out, and in turn, it is not well-modeled by computationally efficient (and traditionally used) pair nonbonded terms.[3,4,6,8,17] Thus, while many CG models are able to capture pair structure and related properties, higher order correlations and cooperative effects are often poorly represented.[18,19] Second, $W$ is a free energy that has a state dependence because the integral in Eq. (1) involves the temperature and volume, and it is not usually clear how this dependence can be captured simply.[20–23] This makes it difficult to transfer the CG potential to states other than the one at which it was parameterized.

In this work, we explore the use of *mean-field* multibody potentials in the development of CG force fields and characterize the extent to which they improve on the multibody and transferability problems for systems involving the solvation of hydrophobic solutes. Specifically, we use "local density" (LD) potentials that assign an energy to a CG site based on the number of neighboring sites of a given type that lie within a predetermined cutoff distance. Such potentials augment the usual pair nonbonded interactions

a)Author to whom correspondence should be addressed. Electronic mail: shell@engineering.ucsb.edu

but remain computationally efficient, scaling similarly in simulation cost. This strategy is inspired by embedded atom and bond order potentials that attempt to capture multibody electronic effects in metal systems.[24–28] Here, however, we generalize the approach in CG systems, describe a systematic parameterization procedure, and test its application to CG implicit solvation models involving idealized alkane-like solutes in aqueous media.

The transferability problem, which refers to a CG forcefield's ability to predict thermophysical properties at states different from those at which it was parameterized, has been characterized by a number of groups.[18–20,22,29–32] Proper transferability is important not because it eliminates the need to re-parameterize the CG model at different states, but because it ensures thermodynamic consistency and validity of the CG model in all statistical–mechanical ensembles.[19] Several attempts have addressed the specific issue of transferability in CG models of aqueous solutions of macromolecular solutes. Mullinax and Noid proposed an extended ensemble approach that parameterizes a single CG model by combining information from an "ensemble" of AA reference simulations at different state points, thus fixing *a priori* the regime of transferability of the CG model in state-point space.[30] Villa, Peter, and van der Vegt used a modified iterative Boltzmann inversion scheme[5] to develop CG models of aqueous solutions of benzene, observing that the use of pair potentials for intermolecular interactions limited the regime of transferability of the models to dilute concentrations.[31] Other recent developments addressing transferability include bulk and local density based corrections to CG forcefields as ways to account for multibody effects not taken into account by CG pair potentials, discussed below.[32–35]

Are there computationally efficient ways to incorporate multibody effects into bottom up CG models, to improve their fidelity and transferability? One approach adds three (or higher) body terms to the CG forcefield. Indeed, Molinero and co-workers used three body Stillinger-Weber[36] potentials to describe hydrogen bonding in a single site CG model of water,[37,38] which has been shown to have excellent accuracy compared to detailed AA water models. While this approach has even been successfully translated to non-bulk scenarios,[39] CG potentials for water might be simple to intuit and implement because of its tetrahedral geometry, whereas general three body potentials for arbitrary interactions may prove conceptually and computationally more difficult to parameterize.[40] Moving towards broader approaches, Voth and co-workers developed a method to systematically parameterize generalized Stillinger-Weber forms within the multiscale coarse-graining force-matching framework, which they also used to create CG models of water.[41] Das and Andersen later proposed an even more general three-body scheme using adaptively applied "multiresolution" functions similar to wavelets to provide a larger basis set for the CG forcefield.[40]

Here, we explore an alternative, mean-field approach to incorporate multibody effects, whereby a particle's energy is modulated by the local density of neighboring CG sites around it. We are inspired by the Embedded Atom Method (EAM) of Daw and Baskes,[42] which was a historical improvement on internuclear CG pair potentials used to model metallic cohesion.[24,42] In this case, the electronic degrees of freedom are coarse-grained out of the picture, but the contribution of the local electronic environment is captured by assigning an effective electron density to each nuclei that gives rise to an "embedding" energy. Such an approach is intrinsically multibody in nature because the embedding energy can depend nonlinearly on the local electron density. At the same time, it is computationally efficient, requiring only two pair interaction loops—one to compute the densities at each nuclei and the other to evaluate energies and forces. Interestingly, Ercolessi and Adams also used similar manybody potentials in their seminal paper that introduced the force-matching algorithm.[2]

We propose to expand the EAM framework to "local density" potentials that can be applied generally to CG models as a simple way to include multibody effects. In this case, a site experiences a local density energy that is modulated by the number of sites of a given type (or types) within a cutoff radius. To parameterize and develop the form of these potentials, we propose to use the relative entropy coarse graining framework,[11,17] which provides a general optimization strategy to minimize the information lost in a CG model, relative to a reference target AA system.

We note several closely related efforts in the literature. Allen and Rutledge proposed global and local density-based corrections to standalone CG pair potentials in constructing implicit solvent models.[33,34] They parameterized the corrections in terms of the excess chemical potential for the transfer of solute groups from a "solvent exposed state to a fully screened environment," since the relative hydrophobicity of a solute depends on the change in chemical potential when passing from a solvent-exposed to a solute-screened state. In addition, Izvekov *et al.* proposed CG models using pair potentials whose corresponding pair forces vary with the average local density of the two interaction sites;[35] the pair forces and potential at each *local* density are determined through force-matching on a system at the same *bulk* density. (We note that, in a very recent work by Moore *et al.*, this CG model was extended to include density dependence through a form of the CG forcefield that conserves energy and is amenable to a dissipative-particle-dynamic treatment.[43]) Finally, Dunn and Noid investigated the effect of global volume dependent corrections to pair CG potentials, determined by matching the ensemble-averaged pressure between the AA and CG representations.[32] Their approach was able to accurately capture the bulk density, compressibility, and pressure in pure liquids like n-heptane and toluene.

It is instructive to compare our local density formalism with the aforementioned flavors of density dependent CG potentials. First, the above methods involve parameterization that happens at the global level (e.g., pair interactions are determined at a fixed bulk density). In the first two approaches, the use of local densities then either corrects[33,34] or reformulates and applies at the local level[35] these globally determined interactions (e.g., pair potentials are selected by a local density). In contrast, the approach that we consider directly optimizes all potentials from statistics of local densities in the reference ensemble, without the need for multiple systems at varying bulk conditions and the

approximations/assumptions needed to translate them to the local level. Second, the use of a mean-field term for the local density potential ensures that, formally, all forces are at most pairwise in computation cost, as shown by Frenkel and Pagonabarraga.[44] In cases where a pair potential is modulated by an average pair local density,[35] instead of using a separate mean-field local density additive term, forces incur three body loops in principle to account for the influence of third-party sites on the local density and hence interactions associated with a given pair. Third, the robustness of the relative entropy minimization framework allows us to simultaneously and generally optimize both the CG pair and the LD potential components of the forcefield, instead of relying on different objective functions for separate construction of the two.[43]

As an application of our approach, we use local density potentials to develop bottom-up implicit aqueous solvation models. Water is a ubiquitous solvent, particularly in biology, and all-atom water in simulations of solvated macromolecules can dominate computational effort,[45–48] making it an attractive target for removal during coarse-graining. In implicit models the effect of solvent is incorporated into the effective solute interatomic interactions, and a wide range of approaches have been proposed.[49–55] The approach here is unique in that we use a bottom-up coarse-graining technique to uncover the form of the potential from reference AA simulations with explicit water. Specifically, we study the hydrophobic collapse of a polymer and the aggregation of small hydrophobes in water, where the water is coarse-grained out entirely.

Water-mediated, and in particular hydrophobic, interactions are critical to many biophysical phenomena, from protein folding to membrane formation,[56–58] and can be highly multibody in nature.[59,60] For example, early studies reported that free energy for trimerization of methanes in water cannot be decomposed into a sum of two-body terms obtained from the dimerization process.[61–64] While there has been some controversy as to whether the three-body effect has a positive[61] or an inhibitive[62,63] (anti-cooperative) effect on methane aggregation, there is evidence that it is non-negligible even for moderately high solute concentration.[64,65] Higher order correlations may also be relevant to electrostatic interactions in water clusters (through underlying polarization effects)[66] and more generally.[67]

Local density potentials are one strategy to capture such multibody effects in implicit solvation models, but they also offer the ability to directly control various particle number fluctuations in the neighborhood of a solute. This point is key as the recent theory[68,69] and simulations[70] suggest that hydrophobic interactions may be understood in terms of fluctuations in the local density of water vicinal to a solute. Indeed, Garde and coworkers have shown that local water density fluctuations are an important signature of molecular hydrophobicity and have theoretical connections[71,72] to compressibility of the solute hydration shell of water molecules. For example, local density fluctuations in water near a solvated polymer directly affect the associated hydration free energy and hence its collapse characteristics.[73–76] Below we explore the extent to which local density potentials can improve on CG models of aqueous solvation of hydrophobic solutes.

The remainder of this paper is organized as follows. Section II presents the mathematical structure of the local density potential and outlines its theoretical connections to multibody effects. Section III uses relative entropy minimization to parameterize these CG models for two hydrophobic solute systems and examines their ability to predict structural metrics, including when transferred to systems of different kinds. Finally, Section IV concludes the paper.

## II. METHODS

### A. Theoretical formulation for local density potentials

For the purposes of illustration, we first consider a CG model consisting of a single type of pseudoatom. In this case, we can measure the local density $\rho_i$ of a site $i$ as the total number of neighboring sites that are within a fixed cutoff $r_c$, using

$$\rho_i = \sum_{j \neq i} \varphi\left(r_{ij}\right), \tag{2}$$

where $\varphi\left(r_{ij}\right)$ is an indicator function that is 1 for neighboring site $j$ when its pair distance $r_{ij}$ is within a cutoff $r_c$. In this manner, $\rho_i$ measures a local coordination number for neighbors around site $i$. In turn, the contribution to the total LD energy, for each such atom $i$, is a (yet unspecified) function of the local density,

$$U_{LD} = \sum_i f\left(\rho_i\right). \tag{3}$$

In practice, $\varphi$ can be a smooth function that quickly but continuously decreases to zero at $r_c$ to ensure the continuity of its first derivative and thus of the interaction forces in a MD simulation. We choose a computationally convenient form that does not require absolute pair distances or square root operations

$$\varphi(r) = \begin{cases} 1 & r \leq r_0 \\ c_0 + c_2\, r^2 + c_4\, r^4 + c_6\, r^6 & r \in (r_0, r_c) \\ 0 & r \geq r_c \end{cases}. \tag{4}$$

Here, the coefficients $\{c\}$ are determined by requiring continuity of $\varphi$ and its first derivative at the "outer" cutoff $r_c$ and at an "inner" cutoff $r_0$ that is slightly smaller. Throughout this paper we maintain $r_0 = r_c - 1.2$ Å,

$$c_0 = \frac{1 - 3r_0^2/r_c^2}{\left(1 - r_0^2/r_c^2\right)^3}, \quad c_2 = \frac{1}{r_c^2}\frac{6r_0^2/r_c^2}{\left(1 - r_0^2/r_c^2\right)^3},$$
$$c_4 = -\frac{1}{r_c^4}\frac{3\left(1 + r_0^2/r_c^2\right)}{\left(1 - r_0^2/r_c^2\right)^3}, \quad c_6 = \frac{1}{r_c^6}\frac{2}{\left(1 - r_0^2/r_c^2\right)^3}. \tag{5}$$

The indicator function is illustrated in Figure 1.

In this approach, the calculation of local densities has a similar computational complexity as pair potentials ($O\left(n^2\right)$, ostensibly, but less with neighbor lists). In practice, it requires two pair loops: the first calculates the local densities at each site, and the second evaluates the energies and pair forces.

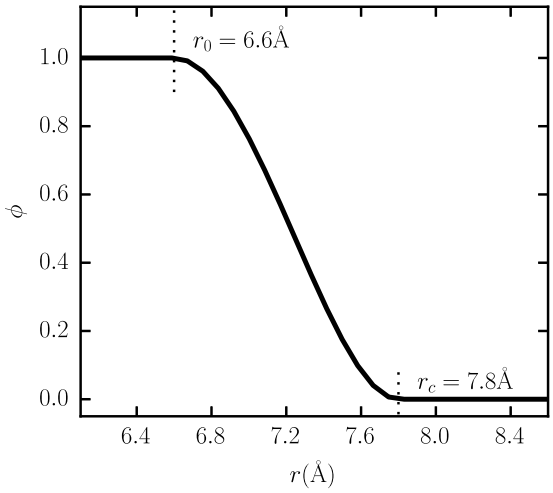


FIG. 1. Indicator function $\phi(r)$ for local density potentials, as given in Eq. (4). $\phi$ goes to zero quickly and continuously between an inner cutoff $r_0$ and an outer cutoff $r_c$. Here $r_0 = r_c - 1.2$ has been chosen.

The complete CG forcefield uses $U_{LD}$ as an additive correction to the traditional two-body pair potentials $u_{pair}$ and can be written as

$$U_{CG} = \sum_{i<j} u_{\text{pair}}(r_{ij}) + \sum_i f(\rho_i). \tag{6}$$

In our approach, we do not specify a specific functional form for the LD potential but represent it as a flexible spline whose coefficients (i.e., knot points) are determined through the process of relative entropy optimization with respect to a reference all-atom ensemble.

For CG models with more than one pseudoatom type, there are multiple ways to define a local density, depending on both the central and neighboring types, and hence it is possible to include several distinct LD potentials. A general formulation of the approach includes an arbitrary number of distinct local densities and associated LD potentials, indexed by a variable $k$,

$$\rho_i^{(k)} = \sum_{j\neq i} b_{\beta(j)}^{(k)} \varphi(r_{ij}) \tag{7}$$

and

$$U_{LD} = \sum_i \sum_k a_{\alpha(i)}^{(k)} f^{(k)}\left(\rho_i^{(k)}\right). \tag{8}$$

Here, $a$ and $b$ are filters for central and neighbor sites, respectively (and are functions of the site atom types), while $\alpha$ and $\beta$ denote the types of atoms $i$ and $j$, respectively: $a_{\alpha(i)}^{(k)}$ is 1 if the central atom $i$ of type $\alpha$ is subject to a LD potential of type $k$ and 0 otherwise. Similarly, $b_{\beta(j)}^{(k)}$ is 1 if the neighboring atom $j$ of type $\beta$ contributes to the local density of type $k$ around site $i$; otherwise it is zero.

With these forms, the forces on sites due to the LD potentials extend, as usual, from the potential gradient. For each LD potential $k$, the expression for the force $\mathbf{f}_i$ on a central atom $i$, due to its neighbors, is as follows, where we have suppressed the superscript $k$ for clarity:

$$\mathbf{f}_i^{(i\text{ central})} = -\nabla_{\mathbf{r}_i} U = -a_{\alpha(i)} \frac{df(\rho_i)}{d\rho} \sum_j b_{\beta(j)} \frac{d\varphi(r_{ij})}{dr} \frac{\mathbf{r}_i - \mathbf{r}_j}{r_{ij}}. \tag{9}$$

This has the form of a pairwise force. The force on central atom $i$ due to neighbor $j$ is

$$\mathbf{f}_{ij}^{(i\text{ central})} = -a_{\alpha(i)} b_{\beta(j)} \frac{df(\rho_i)}{d\rho} \frac{d\varphi(r_{ij})}{dr} \frac{\mathbf{r}_i - \mathbf{r}_j}{r_{ij}} = -\mathbf{f}_{ji}^{(i\text{ central})}. \tag{10}$$

An equal and opposite force applies to atom $j$. However, a *second* pair force arises when $j$ is the central atom and $i$ is the neighbor,

$$\mathbf{f}_{ij}^{(j\text{ central})} = -a_{\beta(j)} b_{\alpha(i)} \frac{df(\rho_j)}{d\rho} \frac{d\varphi(r_{ij})}{dr} \frac{\mathbf{r}_i - \mathbf{r}_j}{r_{ij}} = -\mathbf{f}_{ji}^{(j\text{ central})}. \tag{11}$$

The total pair force that must be added to $i$ and subtracted from $j$ is therefore

$$\mathbf{f}_{ij} = -\left[a_{\alpha(i)} b_{\beta(j)} \frac{df(\rho_i)}{d\rho} + a_{\beta(j)} b_{\alpha(i)} \frac{df(\rho_j)}{d\rho}\right] \times \frac{d\varphi(r_{ij})}{dr} \frac{\mathbf{r}_i - \mathbf{r}_j}{r_{ij}}. \tag{12}$$

Note that the local densities must be computed in a separate, earlier pair loop in order for the forces to be determined.

LD potentials are closely related to excess free energy terms that improve the quality of the CG model, as suggested initially by Frenkel and Pagonabarraga.[44,77] Approximating the corrective effect of the LD potential to the pair-potential as a first order perturbation (meaningful when the correction is weak), its addition to the CG model causes a change in free energy equal to $\Delta A \approx \langle U_{LD}\rangle_{\text{CG,pair}}$, where the subscript indicates an ensemble average in the pair-only CG case. In this sense, the local density potential captures a multibody contribution to the CG free energy that is in addition to the dominant contribution from pair interactions.

### B. Relative entropy coarse-graining

We parameterize the CG forcefield using the information-theoretic coarse-graining framework introduced by Shell.[11,78] Here, the relative entropy, or Kullback-Liebler divergence,[79] quantifies the quality of a putative CG model in comparison to a detailed, reference AA system; one way of expressing it is

$$S_{\text{rel}} = \int p_{AA}(\mathbf{r}) \ln\left(\frac{p_{AA}(\mathbf{r})}{p_{CG}(\mathbf{M}(\mathbf{r}))}\right) d\mathbf{r} + S_{\text{map}}, \tag{13}$$

where $p_{AA}(\mathbf{r})$ gives the equilibrium configurational probability in the AA ensemble, while $p_{CG}(\mathbf{R})$ gives the corresponding CG one. As before, $\mathbf{R} = \mathbf{M}(\mathbf{r})$ is the mapping operation that eliminates atoms or replaces groups of them with center-of-mass sites. The integral proceeds over all AA microstates, although it is possible to reformulate Eq. (13) as an integral in the CG degrees of freedom.[80] $S_{\text{map}}$ is a

mapping entropy that measures the number of distinct AA configurations that map to the same CG one; importantly, it is independent of the CG force field $U_{CG}$ such that it plays no role in the scenarios described here.

The relative entropy measures the information "lost" upon moving from the AA to CG ensemble and is thus strictly zero or positive.[11] Its minimization increases overlap between the two systems and suggests a natural systematic strategy for parameterizing CG models from reference AA systems. Shell and co-workers used this approach to construct single-site CG water models that capture a number of bulk properties and hydrophobic interactions.[81–83] They also showed that the relative entropy is tightly linked to errors incurred upon coarse graining, making it an important measurement for signaling *a priori* the conditions of validity of CG models.[84]

In the canonical ensemble, the relative entropy can be expressed as

$$S_{\text{rel}} = \beta\langle U_{CG}(\boldsymbol{\lambda}) - U_{AA}\rangle_{AA} - \beta\left(A_{CG}(\boldsymbol{\lambda}) - A_{AA}\right) + S_{\text{map}}, \tag{14}$$

where $U_X$ and $A_X$ denote the potential and Helmholtz free energies in ensemble $X = AA$ or CG. The CG quantities are functions of its forcefield parameters $\boldsymbol{\lambda}$, which for the present problem are the unknown coefficients in the cubic spline forms chosen for the pairwise CG potentials $u_{pair}$ and LD potential functions $f(\rho)$. The coarse graining strategy then locates the minimum of $S_{\text{rel}}$ in $\boldsymbol{\lambda}$ space, which is achieved through conjugate-gradient minimization.[17] Because all optimized potentials are represented by splines, and thus all parameters appear linearly in the energy, the relative entropy contains a single basin in such a parameter space.[78] To accelerate the minimization and reduce the number of trial CG MD runs during parameterization, we use the efficient trajectory reweighting and perturbation strategy formulated by Carmichael and Shell that re-uses information from existing CG trajectories.[17]

### C. Test systems and simulation details

Our first test case involves coarse-graining a water-solvated, hydrophobic polymer, as shown in Fig. 2. For the reference AA system, we mimic an alkane-like polymer called "c-25" that was studied by Athawale *et al.*[73] The polymer consists of 25 methane-sized monomers, with diameter 3.73 Å, and equilibrium backbone bond lengths and angles of 1.53 Å and 111°, respectively. Since our primary focus is many-body solvation effects, we study a "superhydrophobic" version of the polymer in which nonbonded monomers interact through Weeks-Chandler-Andersen (WCA)[85] potentials with parameters $\sigma = 3.73$ Å and $\epsilon = 0.139\,86$ kcal/mol, while arithmetic mixing rules are used to evaluate the monomer-water parameters. Harmonic potentials describe bond and angle interactions and are taken from Ref. 73.

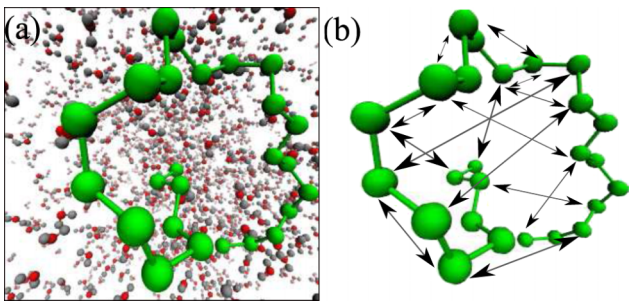


FIG. 2. (a) Reference AA description of the c-25 polymer with 25 methane sized monomeric beads in 1700 water molecules, at 298 K and 1 atm. (b) Implicit solvent CG model of the same system: the waters are coarse-grained away and the polymer-water interactions are then embedded into effective CG potentials between the monomers.

We also investigate a second, comparative case in which we delete all polymer bonds, angles, and associated interactions, to assess the effect of backbone connectivity. Thus, this case consists of 25 independent solvated, superhydrophobic methane-like particles that we term a "methane" system although in reality the WCA potential is unrealistic because it lacks attractive interactions. Later we examine the case of full Lennard Jones interactions in both the c-25 and methane systems, in order to study the effect of solute-solvent attractions on the efficacy of the CG models.

Explicit-water AA simulations at 298 K and 1 atm are carried out with the MD engine LAMMPS,[86] using the SPC/E[87] model of water constrained with the SHAKE algorithm.[88] The simulation for a single 25-mer and 1700 water molecules is first equilibrated for 1 ns in a NPT ensemble using the Parniello-Rahman barostat[89] to determine the equilibrium system volume, followed by a further 2 ns of equilibration under NVT conditions. Trajectory data are then sampled from 26 ns of NVT production time. AA simulations for the methane system involve 2 ns each of NPT and NVT equilibration stages, followed by 30 ns of production.

The CG model for c-25 removes all water molecules, leaving only the single 25-bead polymer, with bond and angle interactions that are retained from the explicit water version. The effect of solvent is then built into effective nonbonded pair and local density potentials that are functions of the inter-monomer pairwise distances and local densities, respectively. Both potentials are represented by flexible cubic splines with unknown coefficients (knot points) that are determined through relative entropy minimization. 40 knot points are used for CG spline pair potentials, while 50 are used for the LD potentials.

For both the polymer and methane systems, we optimize the CG potentials for three different cases that provide instructive comparisons, as summarized in Table I. The pair-spline-only, or SP, approach renormalizes only the nonbonded inter-monomer interactions into an effective pair potential described by a B-spline; this is perhaps the conventional approach to implicit solvent CG interactions. The pair spline and local density (SPLD) approach not only renormalizes the nonbonded interactions but also determines the form of a local density potential based on the number of neighboring monomers surrounding each central one. Finally, the local-density-only case, LD, keeps the WCA pair interactions from the AA system intact as the pair potential and embeds all effects of solvation into a local density potential. SP and SPLD, therefore, serve as negative and positive controls to tease out the relative contribution of the LD potential, while

TABLE I. Comparison of and nomenclature for different coarse graining strategies and controls.

| CG strategy | Bonded interactions | Pair interactions | Local density interactions |
|---|---|---|---|
| SP | Same as AA | $S_{\text{rel}}$ optimized spline | None |
| SPLD | Same as AA | $S_{\text{rel}}$ optimized spline | $S_{\text{rel}}$ optimized spline |
| LD | Same as AA | Same as AA | $S_{\text{rel}}$ optimized spline |

the LD-only case tests its capability as a single mean field representation of the complete implicit solvent force field. Note that the control strategy, LD, should not be confused with the acronym LD used to abbreviate the local density potential throughout the paper.

## III. RESULTS AND DISCUSSION

### A. CG model of c-25

We parameterize the CG c-25 polymer through relative entropy optimization with a LD cutoff of $r_c = 7.8$ Å, using the three different coarse-graining routes of Table I. Here, the relevant local density is the number of monomers within a range $r_c$ from a central monomer. This cutoff is an important free parameter of the CG model, but before discussing its determination, we first provide some illustrative results from the relative entropy minimization procedure.

Fig. 3 shows the final LD potential and distribution for the SPLD case. First, we note that the LD potential decreases with the local density ($\Delta U_{LD} \sim -1.0$ kcal/mol over the full range of the density), thus favoring aggregation of the individual monomers and collapse of the polymer into a compact state, consistent with the idea that the water induces an effective inter-bead attraction of these hydrophobic units. The LD potential is constant for densities less than 5, ultimately due to bond length constraints; each monomer always has a local coordination number of at least 4 due to neighboring bonded monomers and the chosen cutoff length. Above 5, the LD potential sharply decreases, but its effect then weakens

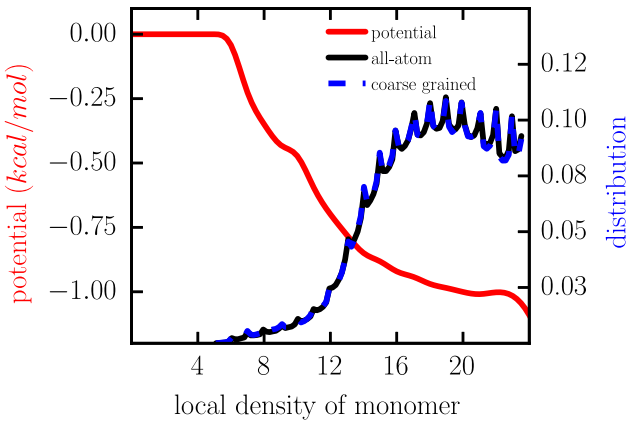


FIG. 3. Comparison of the local density distribution of the CG polymer for the SPLD case, in which both the LD potential and a CG splined pair potential are optimized with respect to the AA system. The LD potential (shown in red) decreases with greater local crowding around the CG monomers, thus favoring collapse of the polymer chain.

beyond a coordination of 13-14. The high-density behavior is expected to flatten, as the influence of additional species diminishes when a full coordination shell around the central particle already exists within the cutoff. Formally, the LD spline is forced to have a zero slope beyond the maximum possible density of 24 (although this is not obvious from the figure), since there is no information in the AA reference to lead to parameterization there.

Interestingly, if we compare the spline pair potentials determined with (SPLD case) and without (SP case) the support of a LD potential (see Figs. S1, S2, and S3 in supplementary material), we find that the former are slightly more repulsive and less attractive; the well-depth decreases from 0.11 to 0.04 kcal/mol for the c-25 CG model. This is to be expected because the LD potential shares the net attractive many-body effect of the monomers which otherwise is sustained entirely by the pair potentials of the SP model. In both cases, however, the inter-monomer pair correlation functions near-exactly reproduce the all-atom one, as is expected from the relative entropy minimization procedure in conjunction with spline potentials.[78]

In addition, we observe that the local density distribution from the reference AA system is exactly reproduced by the LD-corrected CG forcefield. Arguably, it is important to faithfully reproduce this distribution in an aqueous implicit solvent, since the solute local density fluctuations are anti-correlated with the local water density fluctuations, which in turn strongly influence the hydration free energy of hydrophobic units.[68,72,74] Here, the optimization procedure guarantees that the AA and CG local density distributions should match near-exactly at a relative entropy minimum because flexible splines are used for the LD potential.[78] Interestingly, the LD distribution is peaked and skewed around a local density of 20, which suggests that the polymer coils into tightly folded conformations. The jagged peaks throughout the upper contour of the distribution are due to the semi-discrete nature of the indicator function $\varphi(r)$ that is used to determine the local density. If $\varphi(r)$ were a true Heaviside step function, the distribution would involve weighted delta functions at each integer value for the local density; because we use a smooth version (Eq. (4)), the distribution is continuous but still shows some of the sharp-peaked character.

We determine the LD cutoff $r_c$, introduced in the local density indicator function (Eq. (4)), separately from the spline knots that govern the force field potential energies. To fix $r_c$, we exploit the property[11,84] that optimal CG forcefield parameters should minimize the relative entropy between the CG model and its reference AA system. Starting with an initial choice for $r_c$, we minimize the relative entropy $S_{\text{rel}}$ in the space of the other force field parameters $\boldsymbol{\lambda}$; let their final,

optimal values be $\boldsymbol{\lambda}^*$. Then, the variation of the minimized relative entropy with $r_c$ follows:

$$\frac{dS_{\rm rel}}{dr_c} = \left(\frac{\partial S_{\rm rel}(\boldsymbol{\lambda}^*, r_c)}{\partial r_c}\right)_{\boldsymbol{\lambda}} + \left(\frac{\partial S_{\rm rel}(\boldsymbol{\lambda}^*, r_c)}{\partial \boldsymbol{\lambda}}\right)_{r_c}\left(\frac{d\boldsymbol{\lambda}}{dr_c}\right) = \left(\frac{\partial S_{\rm rel}(\boldsymbol{\lambda}^*, r_c)}{\partial r_c}\right)_{\boldsymbol{\lambda}}, \quad (15)$$

where the second term vanishes because $\boldsymbol{\lambda}^*$ is determined by $\frac{\partial S_{rel}}{\partial \boldsymbol{\lambda}}\Big|_{\boldsymbol{\lambda}=\boldsymbol{\lambda}^*} = 0$.[11] We integrate Eq. (15) to determine the dependence of $S_{\rm rel}$ on the cutoff by finely discretizing $r_c$ in the range 4-10 Å. The change in relative entropy $\Delta S_{{\rm rel},1\to2}$ from one cutoff ($r_{c,1}$) to the next ($r_{c,2}$) is evaluated by re-casting Eq. (13) as

$$\Delta S_{{\rm rel},1\to2} = \beta\left\langle U_{CG}(\boldsymbol{\lambda}_2^*, r_{c,2}) - U_{CG}(\boldsymbol{\lambda}_1^*, r_{c,1})\right\rangle_{AA} - \beta\left(A_{CG}(\boldsymbol{\lambda}_2^*, r_{c,2}) - A_{CG}(\boldsymbol{\lambda}_1^*, r_{c,1})\right), \quad (16)$$

where $\boldsymbol{\lambda}_{\mathbf{k}}^*$ refers to the optimal set of forcefield parameters that minimize $S_{\rm rel}$, which we separately evaluate for each cutoff $r_{c,k}$. The average energy difference $\left\langle U_{CG}(\boldsymbol{\lambda}_2^*, r_{c,2}) - U_{CG}(\boldsymbol{\lambda}_1^*, r_{c,1})\right\rangle_{AA}$ is then computed by re-processing AA trajectories and using the optimized CG parameters, while the free energy difference $A_{CG}(\boldsymbol{\lambda}_2^*, r_{c,2}) - A_{CG}(\boldsymbol{\lambda}_1^*, r_{c,1})$ is estimated using MD simulations of the two CG models and the Bennett acceptance ratio method.[90]

Fig. 4(a) shows that the ($S_{\rm rel}$, $r_c$) space for the polymer-water system is approximately concave and admits two local minima near 6.5 and 7.8 Å, respectively. This $S_{\rm rel}$ landscape does not guarantee a single minimum[78] (as discussed earlier in Section II B), since it depends on $r_c$ which affects the CG forcefield in a non-linear manner. Note that this figure is essentially a projection of the higher dimensional space $S_{\rm rel}(\boldsymbol{\lambda}, r_c)$ along the $r_c$ coordinate with $\boldsymbol{\lambda} = \boldsymbol{\lambda}^*(r_c)$. Apparent statistical noise in the calculated relative entropy likely stems from the determination of $\boldsymbol{\lambda}^*(r_c)$, which involves a lengthy optimization in the high-dimensional $\boldsymbol{\lambda}$ space separately at each cutoff value. Figure 4 shows that low or high LD cutoffs, which stray away from twice the diameter of a monomer, lead to higher relative entropy values and signal a smaller role for the LD potential to improve the CG forcefield. Intuitively, both extremes of cutoffs are undesirable: very low values fail to capture relevant local structures and interactions near a central monomer, while too high values wash out these interactions with irrelevant "bulk" fluctuations that are far away. We pick a cutoff at 7.8 Å which, within the noise of the calculations, seems to be near a global minimum in $S_{\rm rel}$.

It is instructive to note that the two minima of Fig. 4 embed information about the hydration shell structure around the monomers. In particular, the minimum at smaller distances captures the first hydration shell and seems to produce local monomer densities that are correlated with the number of hydration shell waters. To quantify this connection, we calculate the correlation coefficient between the instantaneous number of first hydration shell waters (water-monomer distance less than 5.6 Å) and the instantaneous local density of monomers around monomers, on a frame-by-frame basis across the entire AA trajectory. Fig. 4(b) shows that the squared correlation coefficient ($R^2$) has a maximum at

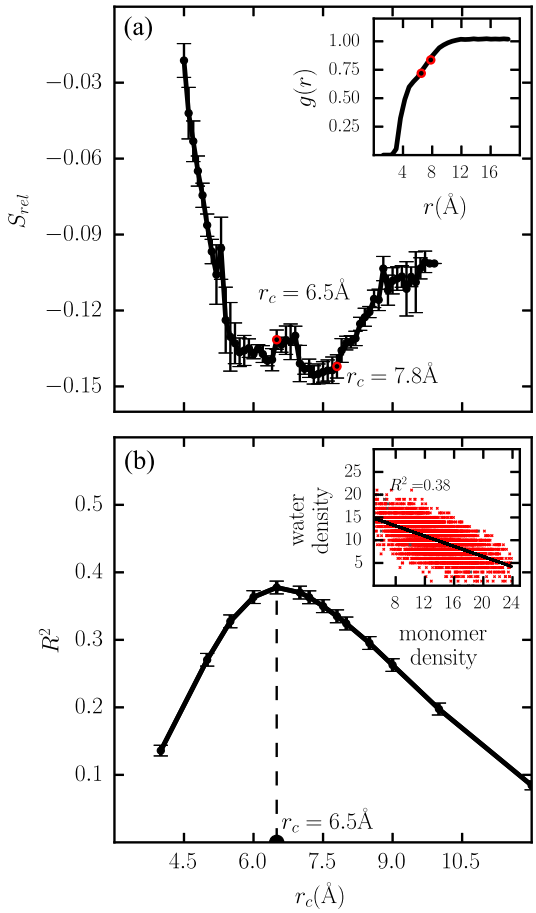


FIG. 4. (a) Selection of the local density cutoff ($r_c$) that minimizes the relative entropy $S_{rel}$. The local minimum near 6.5 Å is related to the first shell of the monomer-water radial distribution function, while the minimum at 7.8 Å includes part of the second shell (inset). Note that the relative entropy is shifted such that its value at the lowest cutoff is zero. (b) The correlation between monomer local density and the number of first shell waters (bivariate scatter plot in inset) also peaks around a cutoff of 6.5 Å.

$r_c = 6.5$ Å. While the correlation is not extremely high (maximum at $R^2 = 0.38$), it is still encouraging that some information from water density fluctuations is incorporated in the monomer local density distribution, which in turn bodes well for its ability to capture features of hydrophobic interactions.[68]

Admittedly, constructing the entire ($S_{\rm rel}$, $r_c$) space requires a significant effort involving many relative entropy optimizations and CG model free energy calculations. On the other hand, evaluating the correlation of monomer local density with vicinal water density is a far simpler calculation using the reference AA trajectory that can be obtained prior to parameterizing the CG model. It also seems intuitive to infer the monomer local density from simple structural metrics of the surrounding water. However, the correlation approach is based on the monomer-water two-body radial distribution functions that may neglect higher order interparticle structural correlations of the type that the local density potential is designed to treat. Therefore, finding the minimum of $S_{\rm rel}$ with respect to $r_c$ is likely to be a more robust approach to selecting the cutoff.

### B. Fidelity of the c-25 CG model in reproducing macromolecular properties

To benchmark the accuracy of the optimized c-25 CG model, we compare distributions of several structural metrics to those of the reference AA system, as shown in Fig. 5. In particular, the radius of gyration, $Rg$, and end-to-end distance, $R_{EE}$, are important characterizers of polymer dimension and are often related to the total number of monomeric units through simple scaling laws that elucidate both intra polymer and polymer-solvent interactions. Figs. 5(a) and 5(b) show that including the LD potential in the CG forcefield helps to reproduce the peaks of the distributions (4.2 Å for $R_g$ and 6 Å for $R_{EE}$), while only renormalizing the CG pair potential without a LD contribution, as in the SP case, leads to a model that deviates more notably.

Fig. 5(c) shows that the distribution of per-monomer solvent-accessible-surface-area (SASA), computed with the Shrake-Rupley algorithm,[91] agrees equally well with the all-atom reference for the three CG cases, such that the LD potential has a smaller impact on its behavior. It is worthwhile to note that SASA is a popular proxy[59,92] for the hydrophobic effect in the construction of implicit solvent models, but is expected to break down for very small solutes where hydration free energies scale with volume, not area, and show significant entropic driving forces.[83,93,94] Here the SASA distribution in Fig. 5(c) has peaks around 0 and 30 Å$^2$, and a steady low tail from 50 to 80 Å$^2$. The two (inner) peaks represent CG monomers that are heavily shielded from the solvent and are suggestive of tightly coiled conformations driven by hydrophobic collapse; the first peak at very low degrees of exposure stems from mid-chain monomers that have a large number of nearby neighbors due to the short bond length (note that the bond length is less than half of the monomer diameter). Thus the presence of this peak is representative of the overall coiled structure of the WCA polymer, while its proximity to zero likely reflects significant burial of monomers due to the disparity in bond length and monomer size. The near-constant values of the distribution towards higher values of SASA may be attributed to the fact that the polymer occasionally adopts a structure in which one end of the chain is collapsed, while the other projects in an extended form into the solvent. To quantify this behavior, we compute the coefficient of relative shape anisotropy, given by

$$\kappa = \frac{3}{2}\frac{\lambda_x^4 + \lambda_y^4 + \lambda_z^4}{\left(\lambda_x^2 + \lambda_y^2 + \lambda_z^2\right)^2} - \frac{1}{2}, \tag{17}$$

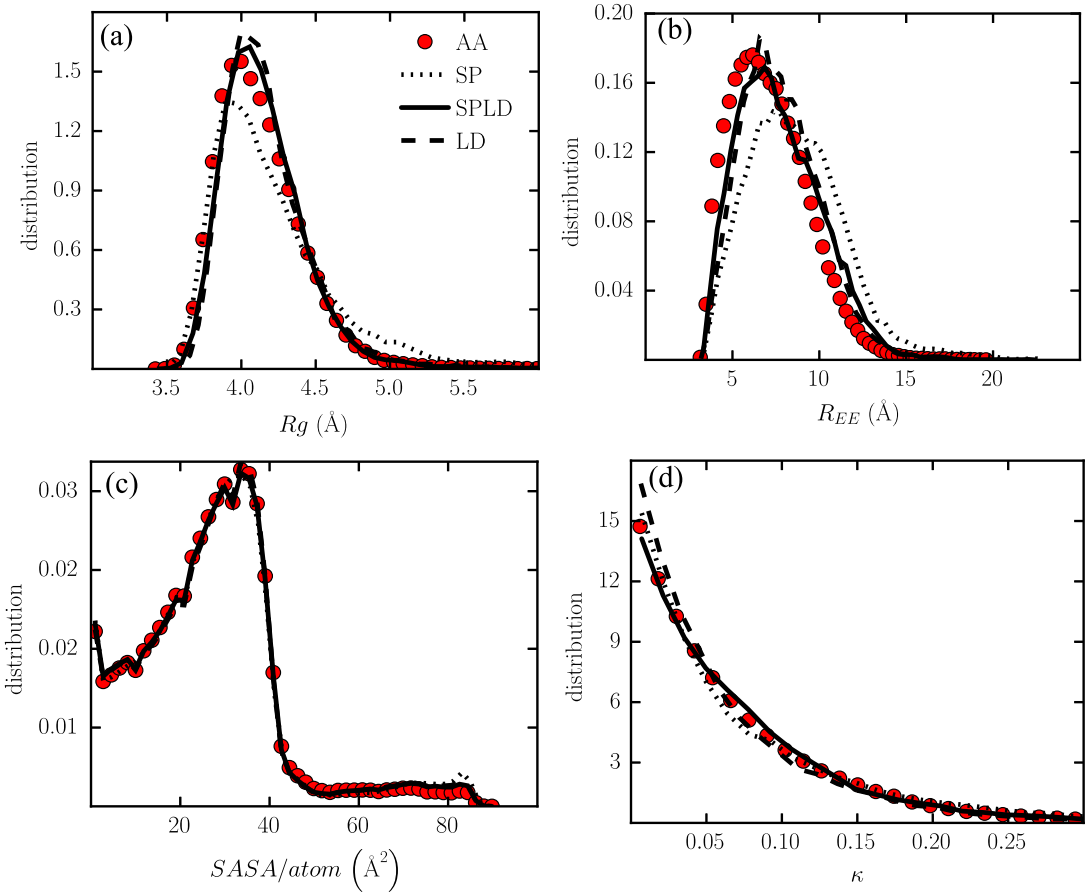


FIG. 5. Comparison of shape metrics between the AA and the CG polymer systems with different nonbonded CG potentials: CG splined pair potentials (SP), CG splined pair potentials with LD correction (SPLD), and LD potential with the original AA nonbonded interactions (LD). Distributions of (a) radius of gyration $Rg$ and (b) end-to-end distance $R_{EE}$ demonstrate that including the LD potential in the CG forcefield improves representation of the AA system. On the other hand, the distributions of (c) per-atom Solvent-Accessible-Surface-Area (SASA) and (d) coefficient of relative anisotropy $\kappa$ show less sensitivity to the form of the CG potentials. Using block average analysis, the average relative errors for these distributions (averaged over the range of the shape metrics near the histogram peaks and across the different CG models, and reported as a fraction of the plotted mean value) are (a) 17.6%, (b) 12%, (c) 6%, and (d) 12.6%. The order-parameter averaged uncertainties are relatively similar for the different CG models.

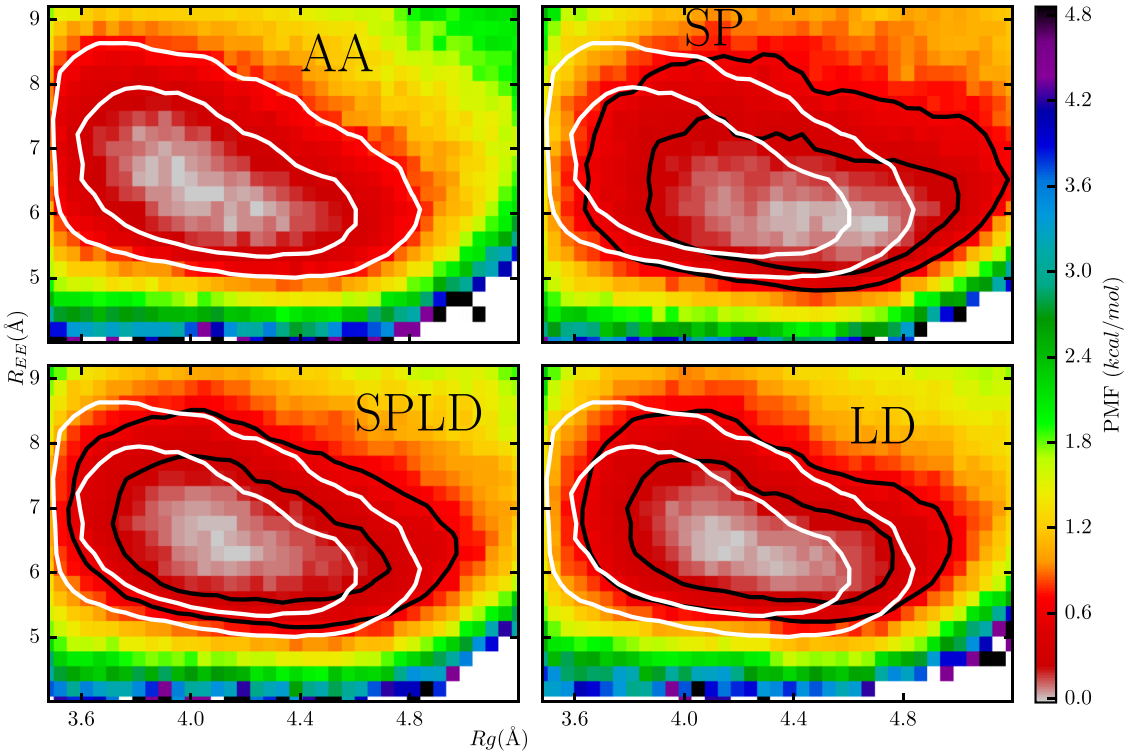


FIG. 6. Free energy of polymer collapse as a function of the end-to-end distance ($R_{EE}$) and radius of gyration ($Rg$) for the AA system compared to the three CG cases: SP, SPLD and LD. The red basins are the regions of most probable conformations, and the contours are shown for 0.5 $k_BT$ and $k_BT$ above the minimum. White contours indicate the AA system and black lines denote the different CG cases. Using block average analysis, the average relative error for the PMFs within the inner contour (as a fraction of the plotted mean value) is 21%. The average errors within the inner contour are relatively similar for the different CG models.

where $\lambda_i$'s are the mutually orthogonal components of the gyration tensor. $\kappa \in [0,1]$ and a value closer to 0 implies greater symmetry, or an overall collapsed conformation, while larger values typically allude to more linear chains. The distributions of $\kappa$ in Fig. 5(d) show that, while the predominant structures are globular and spherical in nature, there are still notable fluctuations to asymmetric configurations of the type described above. The addition of local density

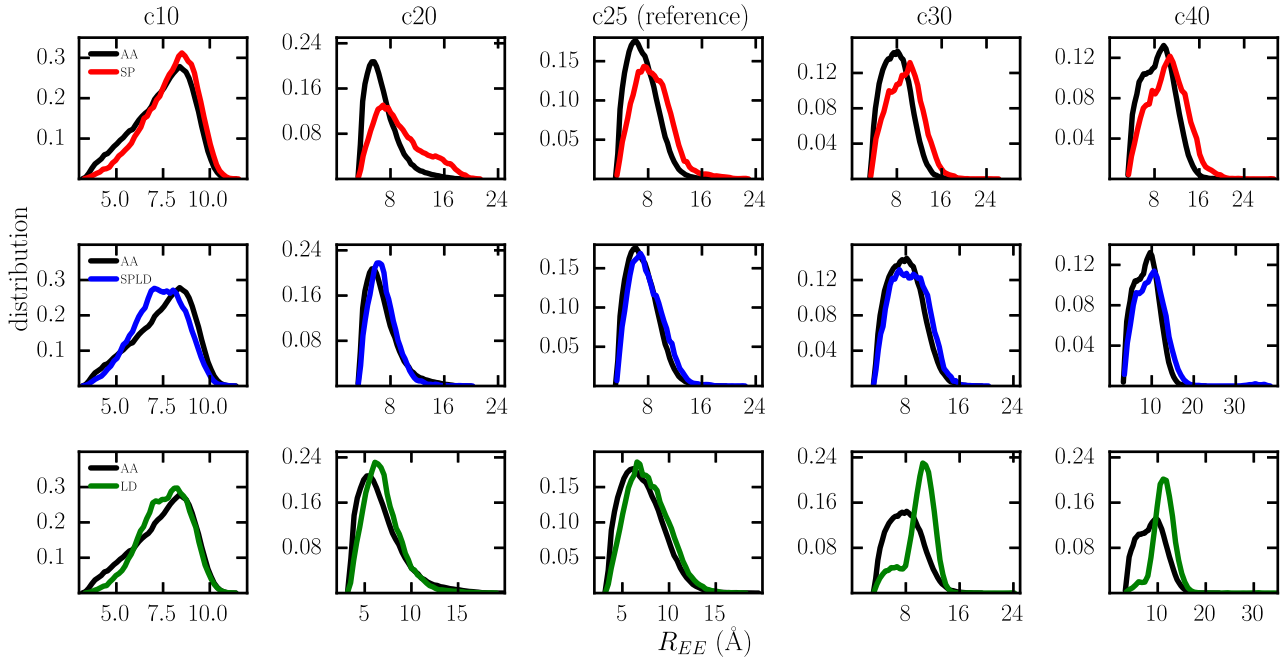


FIG. 7. End-to-end distance ($R_{EE}$) transferability of the CG forcefield parameterized from the 25-mer, for the three different CG-ing schemes: SP, SPLD, and LD. Including LD potentials (SPLD) apparently makes the forcefield more robust than pure CG pair potentials (SP) for chain lengths both smaller (10- and 20-mers) and larger (30- and 40-mers) than the reference.

potentials in the SPLD case shows just slight improvement over the SP scenario in reproducing this distribution. On the other hand, not including renormalized pair interactions (LD case) seems to weaken the quality of the CG model.

Overall, the metrics in Fig. 5 show that the SPLD strategy improves the quality of the CG model relative to the SP case. The LD potential alone performs similarly if slightly worse than the combined SPLD case, as it overestimates several distribution peaks. Thus it may be the case that the functionality of an LD potential as a proxy for an implicit solvation energy, which is a mean-field multibody term, is improved when detailed (non-mean-field) pair interactions between monomers are renormalized in the coarse graining process.

Fig. 6 illustrates the coupling between the $Rg$ and $R_{EE}$ distributions in the form of a free energy surface, where a clear minimum is evident that corresponds to a globular, collapsed state. The region within one $k_BT$ extends roughly from 3.5 to 4.8 Å in $Rg$ and 5.5 to 8.5 Å in $R_{EE}$ for the explicit water (AA) reference. The low $Rg$ end of the basin (≈3.5 to 3.75 Å), where one might expect more significant multibody effects, is not well-captured by the SP approach, which shifts the entire basin to higher values. Both the SPLD and LD-only forcefields appear more successful in reproducing the extents of the basin as visualized through the contours in Figure 6. However, both cases also slightly extend the basin to higher $R_g$ values.

### C. Transferability of the c-25 CG forcefield

Another measure of the success of a CG forcefield is its transferability to systems beyond those at which the model was parameterized, which indirectly assesses whether or not it captures "true" driving forces in a physically realistic manner or is simply an effective fit to the original AA reference. Here, we explore transferability to different chain lengths, between 10 and 40 monomers (denoted by "c-10" to "c-40"). We perform explicit-water MD simulations for each polymer with the same pressure and temperature conditions as c-25 and then compare structural metrics obtained from these AA trajectories to CG simulations based on the c-25 forcefield.

Figs. 7 and 8 show the transferability of the c-25-parameterized potentials in terms of the $R_{EE}$ and $Rg$ distributions, respectively. Overall, the SPLD potential seems marginally more transferable than the other CG cases. Specifically, it provides a better estimate of the distributions at low and moderately high chain lengths (10, 20, 30) for both the shape metrics, but it does underestimate the peak value of the $Rg$ distribution for the 40-mer. This limit in transferability for $Rg$ at higher chain lengths is likely because the 40-mer explores regimes of local densities that are beyond those sampled by the original system; that is, the c-25 SPLD forcefield embeds local density information only up to 25 monomers within the cutoff radius (Fig. 4). Thus, it does not approximate local density interactions for higher chain lengths that are able to sample at or beyond the high local density edge of the original LD potential (right edge of the red curve in Fig. 3). We also note that the bare LD potential (third row in Figs. 7 and 8) shows even more pronounced errors at large chain lengths, which again is likely due to the absence of data for its parametrization in regimes of the higher (than the c-25 case) local densities that are accessible by the longer chain length cases.

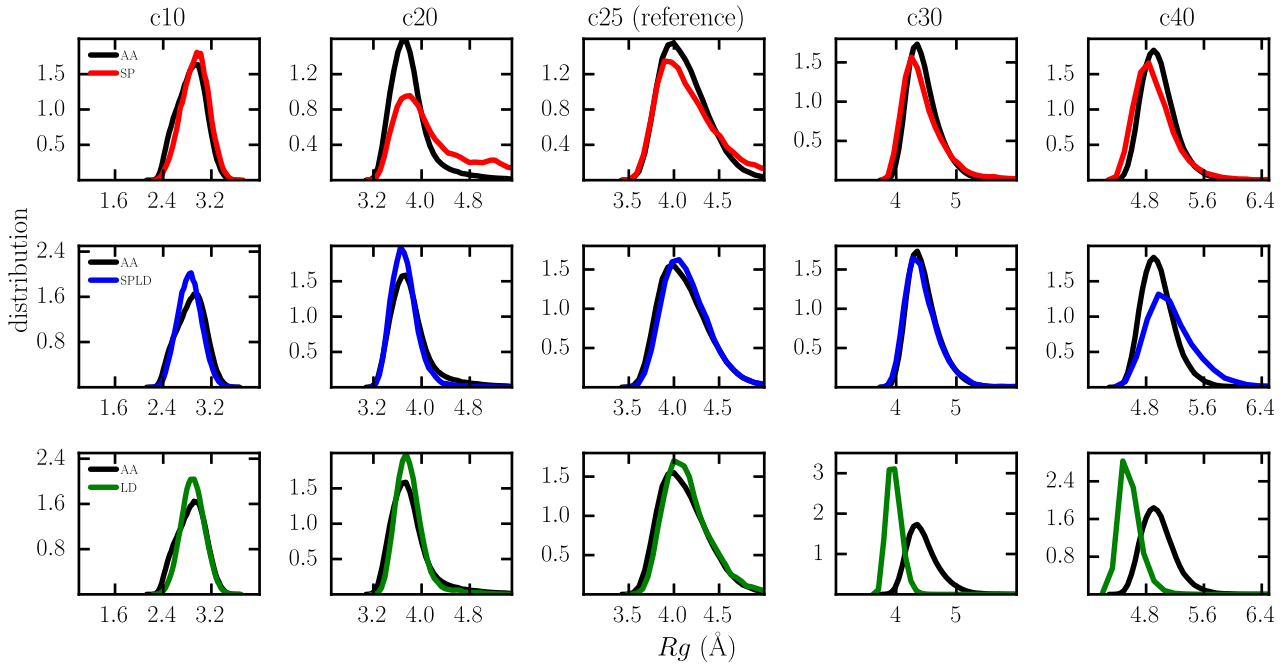


FIG. 8. Radius of gyration ($Rg$) transferability of the CG forcefield parameterized from the 25-mer, for the three different CG-ing strategies. Including the LD potential (SPLD) in the CG forcefield reproduces the $Rg$ distribution faithfully for chain lengths smaller than the reference (10- and 20- mer) but is less representative at state points of high chain length (40-mer).

### D. Relationship to SASA-based implicit solvation

It is worthwhile to examine the relationship between the SPLD implicit solvation strategy and the longstanding tradition of embedding hydrophobic interactions in SASA-based energy terms. Indeed, phenomenological solvation free energies using an effective molecular surface tension with SASA have been a popular choice for modeling macromolecules.[59,92,95–97]

To make the comparison, we examine the parametric relationship between the solvation component of the CG energy and the SASA of individual conformations in the configurational ensemble for c-25. The solvation energy is calculated by subtracting the AA inter-monomer interactions ($U_{WCA}$) from the total effective energy due to the nonbonded part of the SPLD forcefield ($U_{SP} + U_{LD}$), since this provides the effect of the implicit solvent relative to the vacuum interactions. Fig. 9 shows that the solvation energy and SASA have a strong degree of correlation ($R^2 = 0.86$). The slope of this relationship gives an effective interfacial tension between the polymer-water interface at 32 mN/m, which is in relatively good agreement with a previous estimate of 41.5 mN/m for the c-25 system.[73] We perform a similar analysis on other polymer chain lengths, still using the c-25 SPLD force field, and find a 20% variation in the effective interfacial tension; however, it is important to note that these numbers also embed any transferability errors.

### E. CG model of solvated, superhydrophobic methanes

To remove the impact of the polymer architecture and probe "inherent" hydrophobic interactions, we perform comparative simulations in which we delete the bond and angle potentials (Section II C) and construct a system of 25 solvated, superhydrophobic WCA "methanes" that we coarse grain using the SP and SPLD routes.

Our strategy for selecting an appropriate LD cutoff remains similar to the polymer case. Fig. 10 shows the structure of the $(S_{\text{rel}}, r_c)$ space for the methanes, in which two minima at 6.0 and 7.8 Å appear to be equally good choices for the cutoff. Further, as seen in the inset, the first minimum has a strong relationship with the first shell radius of the methane-water radial distribution function and hence, qualitatively conveys information about local water structure. To maintain consistency with the c-25 system, we choose $r_c$ = 7.8 Å for the CG model of implicitly solvated methanes.

Fig. 11 shows the LD potential and LD distributions for the SPLD approach for the methane-water system. As with the polymer in Fig. 3, the LD potential obtained through relative entropy optimization encourages methane aggregation (with an overall change from 0 to ∼15 neighbors, and of

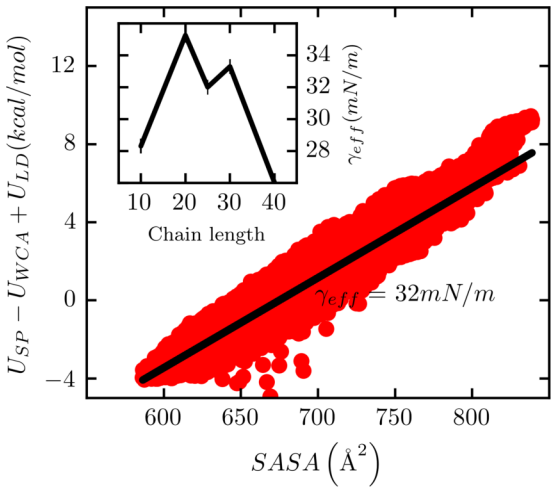


FIG. 9. Correlation of the total solvation energy in the SPLD CG model with the Solvent Accessible Surface Area (SASA) for the c25 polymer. Solvation energy is calculated as $U_{SP} - U_{WCA} + U_{LD}$, where $U_{SP}$ and $U_{LD}$ are intrapolymeric contributions of the CG pair and LD potential parts of the CG forcefield, while $U_{WCA}$ is the energy due to the original all-atom WCA pair intermonomer interactions. An effective interfacial tension given by a linear fit is 32 mN/m, in good agreement with 41.5 mN/m reported by Athawale *et al.*[73] for the c-25 AA system. The inset demonstrates that the effective interfacial tension shows a 20% variation with chain length.

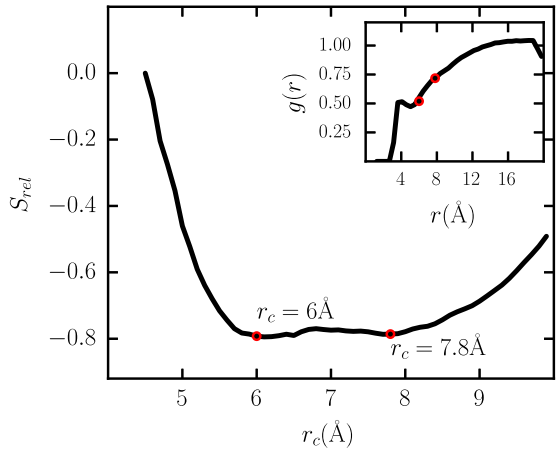


FIG. 10. LD cutoff selection for the assembly of solvated methanes. Here, it is desirable to minimize relative entropy ($S_{\text{rel}}$) as a function of cutoff ($r_c$). Both local minima (6.0 and 7.8 Å) seem equally viable candidates, and the first seems to indicate a cutoff for the first hydration shell radius of the methane-water radial distribution function (inset). Note that the relative entropy has been shifted by its value at the lowest cutoff.

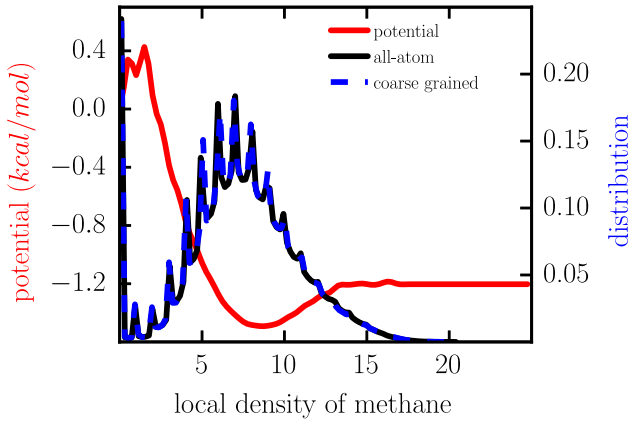


FIG. 11. Comparison of the local density potential (red) and distribution between the CG and AA methane systems. The potential suggests anti-cooperativity for very low local coordination numbers. We have verified, through multiple optimization runs, that the peak structure in this regime is statistically significant (see Fig. S5 in the supplementary material).

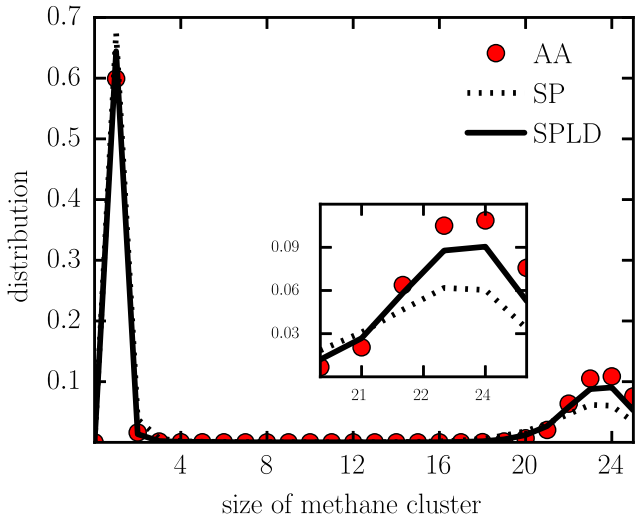


FIG. 12. Distribution of cluster sizes for methane aggregates in water, for different schemes and the reference AA system of 25 solvated methanes. Large size clusters (zoomed inset) are reproduced well only when the LD potential is included with the renormalized CG splined pair potentials (SPLD case). Using block average analysis, the average relative error at the lower peak (as a fraction of the plotted mean value and averaged over the different CG models) is 17%. The average errors near the distribution peak at high cluster size are relatively close for the different CG models.

−1.2 kcal/mol.) However, it shows a slight "repulsive" behavior at very low local densities, where it increases upon the addition of 1-3 neighboring methanes to a lone central one, which is suggestive of anti-cooperativity in low-order assembly. The distribution of local densities from the explicit-water reference is, as expected from relative entropy theory and the use of spline LD potentials, well-matched by the SPLD CG model. The distribution differs from its polymer counterpart (Fig. 3) in terms of the location of a peak near zero local density and another around 7, and in the absence of a tail at high local densities. Both features stem from the ability of the methanes to cluster into a singular, dense aggregate due to the absence of backbone rigidity and bond constraints.

To characterize aggregation in the methane system, we examine the distribution of cluster sizes and make comparisons with that of the explicit water reference simulation. In particular, the cluster distribution can signal cooperative assembly, and the potential for multibody physics to play a role, in the form of marked populations of high-number hydrophobic solute assemblies. Fig. 12 shows that due to strong hydrophobic interactions, the methanes distribute into two phases: a methane-rich phase described by extensive aggregation (cluster size >20) and a water rich phase characterized by sparsely distributed monomers (cluster size ~1). In a larger system, these species would macroscopically phase-separate, but here the total methane number is small and the simulation volume fixed. In comparing the different CG strategies, the SPLD case best replicates the AA distribution and peak at high cluster size showing that the SPLD strategy captures some features of multibody interactions in the aggregate phase, which are not completely described by a pair spline potential alone. It may be noted that the methane cluster observed here is not representative of true methane physics, but rather of the superhydrophobic WCA particles that lack attractive van der Waals interactions.

Fig. 13 highlights the transferability of the CG forcefields in the cluster distributions, using different total methane numbers at the same pressure and temperature. Additional explicit water simulations are carried out with 10, 20, and 30 methanes for comparison. Figure 13 shows the high cluster part of the distribution (similar to the zoomed inset of Fig. 12) for CG simulations using the SP and SPLD forcefields parameterized from the 25 methane case. The SPLD potential shows much better reproduction of the large-size cluster distribution than the SP potential, while the SP potential appears too weak at smaller methane numbers and too strong at higher ones—a possible signature of the need for a multibody potential.

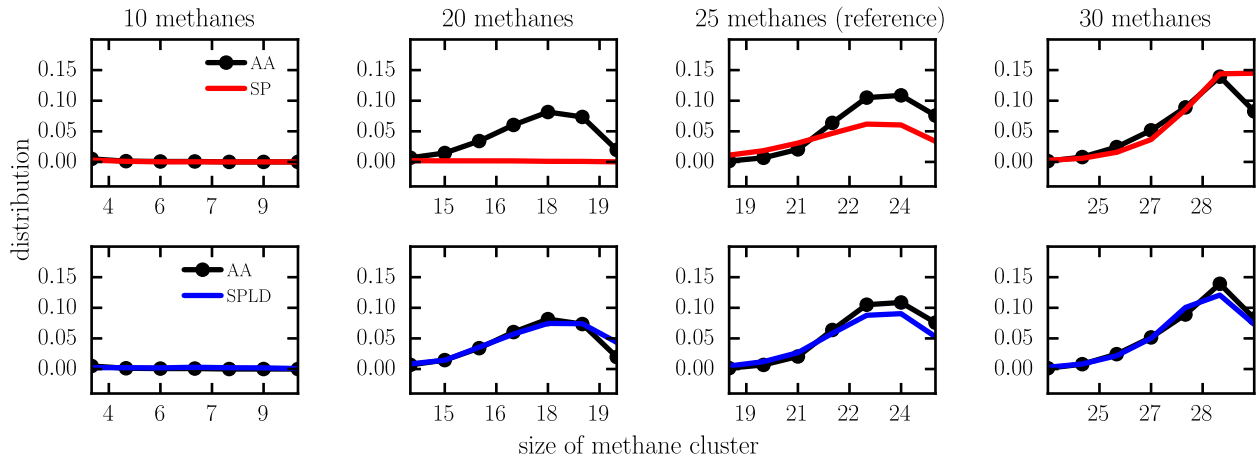


FIG. 13. Cluster size distribution transferability of the CG forcefield parameterized from the system of 25 solvated superhydrophobic (WCA) methanes. The distributions are zoomed to display only the relevant methane-rich phase with large-size clusters. For low methane numbers such as 10, aggregation does not occur. But with increasingly higher methane concentration (20, 30), large size clusters form and are correctly described by the LD-corrected CG forcefield (SPLD). The average relative errors at the distribution peaks (as a fraction of the plotted mean value and averaged over the different CG models) are 13.5% for 10 methanes, 35.5% for 20 methanes, 17% for 25 methanes, and 24.6% for 30 methanes The average errors across the different CG models are quite close.

### F. Effect of attractive hydrophobe interactions

So far, we have investigated solutes that are "superhydrophobic" in nature, described by purely repulsive monomer-monomer and monomer-water WCA interactions, where multibody effects in hydrophobic driving forces should be pronounced. However, it is now well-established that even weak solute-water attractive interactions can produce significant effects and sometimes even qualitatively distinct behavior.[98–100] For a brief comparison, therefore, we characterize the LD approach for the polymer and methane systems when the AA reference model includes a full Lennard-Jones (LJ) potential, with all other conditions unchanged.

Fig. 14 shows the free energy of c-25 as a function of $Rg$ and $R_{EE}$. The basin within roughly 1 $k_BT$ of the minimum represents the region of most probable polymer conformations and is the focus of our analysis. Note that, compared to the PMF for the superhydrophobic polymer (Fig. 6), the basin for the LJ polymer in the AA simulation has a larger $Rg$ (~3.5–5 Å) and smaller $R_{EE}$ (~5–7.5 Å) range. In the CG models, the high end of the basin in $Rg$ is slightly overestimated in all cases. More significant differences exist at the basin's high $R_{EE}$ end, which is overestimated by 13% for the SP and 10% for the SPLD cases but underestimated by roughly 3% for the LD-only case. However, the lowest lying portions of the basin ($\leq$0.5 $k_BT$) seem equally well modeled by each of the CG scenarios, and so the overall differences are not as dramatic as in the superhydrophobic case. It is interesting to note that the LD potential alone, for the attractive polymer, is able to well-describe all of the implicit solvation effects, even without renormalizing the inter-monomer pair potentials.

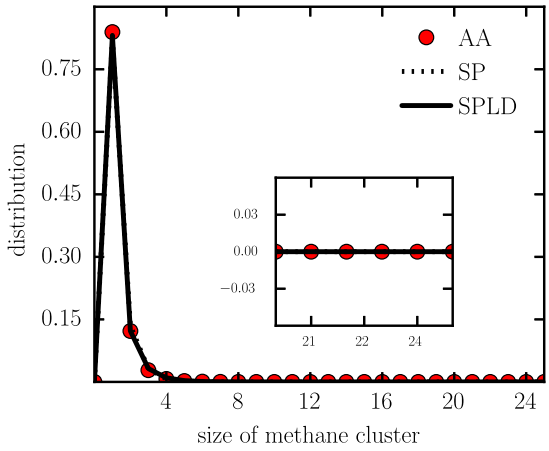


FIG. 15. Distribution of cluster sizes for solvated methanes described by a LJ rather than WCA potential. Weak van der Waals attractions are sufficient to suppress cooperative assembly and manybody interactions, such that both the SP and SPLD techniques collapse on the same distribution, with only a single peak near dispersed methanes. Using block average analysis, the average relative error near the distribution peak (as fraction of the plotted mean value and averaged over the different CG cases) is 8.9%. The average errors for the different CG models are close in magnitude.

For the methane AA system modeled with a LJ potential, the distribution of cluster sizes is less interesting than the WCA case, as shown in Figure 15. One only observes a single peak at a cluster size of 1 implying that the presence of weak solute-water attractions leads to a significant weakening of

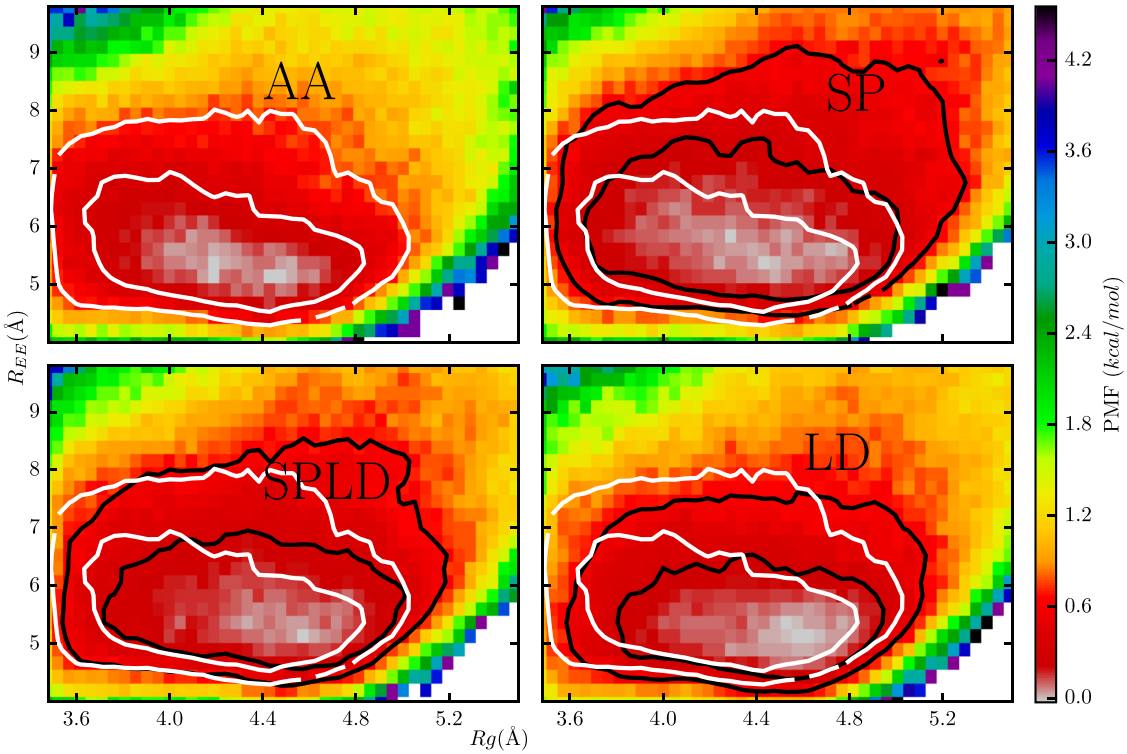


FIG. 14. Free energy of polymer folding as a function of end-to-end distance ($R_{EE}$) and radius of gyration ($Rg$) for a hydrophobic polymer with attractions (LJ rather than WCA potential) using the different CG-ing strategies, SP, SPLD, and LD. The basins represent the regions of most probable conformations (inner and outer contours mark the $0.5k_BT$ and $k_BT$ levels, respectively), and all three CG approaches model the inner contour equally well. White contours indicate the AA system and black lines denote the different CG cases. Using block average analysis, the average relative error for the PMFs within the inner contour (as a fraction of the plotted mean value) for the PMFs is 21%. The average errors within the inner contour among the different CG models are comparable.

hydrophobicity and cooperative self-assembly such that large clusters do not form at all. Both the SP and SPLD potentials, therefore, capture the single methane peak well.

Taken together, the results above show that the addition of local density potentials to CG force fields has a weaker effect on their performance when hydrophobic driving forces for self-assembly are less pronounced. Presumably, in these cases, multibody interactions are weaker in magnitude and most of the effective solvent-mediated attractions can be subsumed into renormalized pair potentials. Interestingly, a local density potential in the polymer case alone does an excellent job of describing the complete solvation effects; this is likely due to the fact that all of the solvent mediated interactions are so weak that they are relative easy to capture with a variety of functional forms (i.e., basis sets) in the CG forcefield.

## IV. CONCLUSION

In this work, we introduced local density (LD) potentials as a simple and computationally fast mean field approach to capturing multibody effects in coarse-grained (CG) models that may improve transferability. While conventional CG models use effective pair potentials to describe nonbonded interactions, such approaches neglect potentially significant multibody effects that naturally arise during the coarse-graining process. LD potentials thus seek to approximate these interactions through an energetic contribution at each site that depends non-linearly on the number of neighbors (of a given type) within a cutoff distance. We have shown that the relative entropy coarse graining framework of Shell and co-workers[11,17,84] offers a systematic and transparent way to fully parameterize LD potentials in CG forcefields, given fully atomistic reference simulations, without needing approximations to adapt global density-dependent potentials at a local molecular level.

The present work also examined the utility of LD potentials in the development of implicit solvation models, with a specific focus on hydrophobic interactions. We selected two examples that demonstrate cooperativity in water-mediated interactions: the collapse of a superhydrophobic polymer and the assembly of superhydrophobic methane-sized particles. In both cases, the addition of a LD potential generally improves the ability of the CG models to capture distributions of structural metrics like radius of gyration and cluster size. At the same time, the LD potential improves the transferability of the CG model to related systems with different polymer lengths or concentrations. In many cases, the optimization of a LD potential alone seemed sufficient to capture the solvent-mediated component of the effective CG force field; however, the optimization of renormalized pair interactions, along with a local density potential, seemed to offer slightly better CG models and transferability. In addition, the superhydrophobic case studies point towards significant multibody interactions that would suggest a role for the LD potential to improve the CG models. However, when the systems are only mildly hydrophobic—accomplished by introducing weak van der Waals solute-water interactions—the improvement afforded by LD potentials is less significant.

It is interesting that such a simple CG potential, based on a single mean-field (the local density), is capable of capturing higher order cooperativity inherent to hydrophobic interactions—without being pre-informed about the microscopic network-forming, tetrahedral, open nature of water structure, or about the unique entropic-enthalpic balance of hydrophobic solvation from a macroscopic point of view. This feature suggests that bottom-up coarse graining techniques using LD and other non-traditional potential forms may offer robust strategies for implicit solvation models that incorporate the hydrophobic effect.[57,60,101] More generally, local density potentials also appear to be a promising tool in the relatively sparse repertoire of methods for developing fast and efficient CG descriptions of phase transitions, where density and concentration-dependent CG interactions are significant. Further, LD potentials can be easily applied to arbitrary CG models of systems, beyond those involving solvation and may have a wide role for improving the ability of CG forcefields to capture multibody effects that emerge as a result of integrating out degrees of freedom.

## SUPPLEMENTARY MATERIAL

See supplementary material for a discussion on the sensitivity of the CG pair potential to the inclusion of a local density field in the CG model.

## ACKNOWLEDGMENTS

We greatly appreciate the support of the National Science Foundation (Award No. CHEM-1300770).

[1]J. C. Palmer and P. G. Debenedetti, AIChE J. **61**, 370 (2015).
[2]F. Ercolessi and J. B. Adams, Europhys. Lett. **26**, 583 (1994).
[3]A. P. Lyubartsev and A. Laaksonen, Phys. Rev. E **52**, 3730 (1995).
[4]F. Müller-Plathe, ChemPhysChem **3**, 754 (2002).
[5]D. Reith, M. Pütz, and F. Müller-Plathe, J. Comput. Chem. **24**, 1624 (2003).
[6]S. Izvekov and G. A. Voth, J. Phys. Chem. B **109**, 2469 (2005).
[7]S. Izvekov and G. A. Voth, J. Chem. Phys. **123**, 134105 (2005).
[8]W. G. Noid, J.-W. Chu, G. S. Ayton, V. Krishna, S. Izvekov, G. A. Voth, A. Das, and H. C. Andersen, J. Chem. Phys. **128**, 244114 (2008).
[9]J. F. Rudzinski and W. G. Noid, Eur. Phys. J.: Spec. Top. **224**, 2193 (2015).
[10]J. F. Dama, A. V. Sinitskiy, M. McCullagh, J. Weare, B. Roux, A. R. Dinner, and G. A. Voth, J. Chem. Theory Comput. **9**, 2466 (2013).
[11]M. S. Shell, J. Chem. Phys. **129**, 144108 (2008).
[12]V. Rühle, C. Junghans, A. Lukyanov, K. Kremer, and D. Andrienko, J. Chem. Theory Comput. **5**, 3211 (2009).
[13]J. G. Kirkwood, J. Chem. Phys. **3**, 300 (1935).
[14]F. H. Stillinger and T. A. Weber, Phys. Rev. A **25**, 978 (1982).
[15]A. Liwo, R. Kaźmierkiewicz, C. Czaplewski, M. Groth, S. Ołdziej, R. J. Wawak, S. Rackovsky, M. R. Pincus, and H. A. Scheraga, J. Comput. Chem. **19**, 259 (1998).
[16]C. N. Likos, Phys. Rep. **348**, 267 (2001).
[17]S. P. Carmichael and M. S. Shell, J. Phys. Chem. B **116**, 8383 (2012).
[18]M. E. Johnson, T. Head-Gordon, and A. A. Louis, J. Chem. Phys. **126**, 144509 (2007).
[19]W. G. Noid, J. Chem. Phys. **139**, 090901 (2013).
[20]J. Ghosh and R. Faller, Mol. Simul. **33**, 759 (2007).
[21]E. Sobolewski, M. Makowski, S. Ołdziej, C. Czaplewski, A. Liwo, and H. A. Scheraga, Protein Eng., Des. Sel. **22**, 547 (2009).
[22]V. Krishna, W. G. Noid, and G. A. Voth, J. Chem. Phys. **131**, 024103 (2009).
[23]A. Das and H. C. Andersen, J. Chem. Phys. **132**, 164106 (2010).
[24]M. S. Daw, S. M. Foiles, and M. I. Baskes, Mater. Sci. Rep. **9**, 251 (1993).
[25]J. Tersoff, Phys. Rev. B **37**, 6991 (1988).
[26]D. W. Brenner, Phys. Rev. B **42**, 9458 (1990).
[27]M. W. Finnis and J. E. Sinclair, Philos. Mag. A **50**, 45 (1984).

[28]J. F. Justo, M. Z. Bazant, E. Kaxiras, V. V. Bulatov, and S. Yip, Phys. Rev. B **58**, 2539 (1998).
[29]A. A. Louis, J. Phys.: Condens. Matter **14**, 9187 (2002).
[30]J. W. Mullinax and W. G. Noid, J. Chem. Phys. **131**, 104110 (2009).
[31]A. Villa, C. Peter, and N. F. A. van der Vegt, J. Chem. Theory Comput. **6**, 2434 (2010).
[32]N. J. H. Dunn and W. G. Noid, J. Chem. Phys. **143**, 243148 (2015).
[33]E. C. Allen and G. C. Rutledge, J. Chem. Phys. **128**, 154115 (2008).
[34]E. C. Allen and G. C. Rutledge, J. Chem. Phys. **130**, 034904 (2009).
[35]S. Izvekov, P. W. Chung, and B. M. Rice, J. Chem. Phys. **135**, 044112 (2011).
[36]F. H. Stillinger and T. A. Weber, Phys. Rev. B **31**, 5262 (1985).
[37]V. Molinero and E. B. Moore, J. Phys. Chem. B **113**, 4008 (2009).
[38]J. Lu, Y. Qiu, R. Baron, and V. Molinero, J. Chem. Theory Comput. **10**, 4104 (2014).
[39]B. C. Knott, V. Molinero, M. F. Doherty, and B. Peters, J. Am. Chem. Soc. **134**, 19544 (2012).
[40]A. Das and H. C. Andersen, J. Chem. Phys. **136**, 194114 (2012).
[41]L. Larini, L. Lu, and G. A. Voth, J. Chem. Phys. **132**, 164107 (2010).
[42]M. S. Daw, Phys. Rev. B **39**, 7441 (1989).
[43]J. D. Moore, B. C. Barnes, S. Izvekov, M. Lísal, M. S. Sellers, D. E. Taylor, and J. K. Brennan, J. Chem. Phys. **144**, 104501 (2016).
[44]I. Pagonabarraga and D. Frenkel, Mol. Simul. **25**, 167 (2000).
[45]E. J. Arthur and C. L. Brooks, J. Comput. Chem. **37**, 927 (2016).
[46]J. T. King, E. J. Arthur, C. L. Brooks, and K. J. Kubarych, J. Am. Chem. Soc. **136**, 188 (2014).
[47]B. R. Brooks, C. L. Brooks, A. D. Mackerell, L. Nilsson, R. J. Petrella, B. Roux, Y. Won, G. Archontis, C. Bartels, S. Boresch, A. Caflisch, L. Caves, Q. Cui, A. R. Dinner, M. Feig, S. Fischer, J. Gao, M. Hodoscek, W. Im, K. Kuczera, T. Lazaridis, J. Ma, V. Ovchinnikov, E. Paci, R. W. Pastor, C. B. Post, J. Z. Pu, M. Schaefer, B. Tidor, R. M. Venable, H. L. Woodcock, X. Wu, W. Yang, D. M. York, and M. Karplus, J. Comput. Chem. **30**, 1545 (2009).
[48]I. T. E. Cheatham and P. A. Kollma, J. Mol. Biol. **259**, 434 (1996).
[49]B. Roux and T. Simonson, Biophys. Chem. **78**, 1 (1999).
[50]T. Lazaridis and M. Karplus, Proteins: Struct., Funct., Bioinf. **35**, 133 (1999).
[51]N. A. Baker, D. Sept, S. Joseph, M. J. Holst, and J. A. McCammon, Proc. Natl. Acad. Sci. U. S. A. **98**, 10037 (2001).
[52]A. Onufriev, D. A. Case, and D. Bashford, J. Comput. Chem. **23**, 1297 (2002).
[53]C. J. Fennell, C. Kehoe, and K. A. Dill, J. Am. Chem. Soc. **132**, 234 (2010).
[54]C. J. Fennell, C. W. Kehoe, and K. A. Dill, Proc. Natl. Acad. Sci. U. S. A. **108**, 3234 (2011).
[55]Y. Wang, J. K. Sigurdsson, E. Brandt, and P. J. Atzberger, Phys. Rev. E **88**, 023301 (2013).
[56]W. Kauzmann, Adv. Protein Chem. **14**, 1 (1959).
[57]C. Tanford, *The Hydrophobic Effect: Formation of Micelles and Biological Membranes* (Wiley, New York, 1973).
[58]K. A. Dill, S. B. Ozkan, M. S. Shell, and T. R. Weikl, Annu. Rev. Biophys. **37**, 289 (2008).
[59]G. Hummer, J. Am. Chem. Soc. **121**, 6299 (1999).
[60]G. Hummer, S. Garde, A. E. Garcí a, and L. R. Pratt, Chem. Phys. **258**, 349 (2000).
[61]C. Czaplewski, S. Rodziewicz-Motowidlo, A. Liwo, D. R. Ripoll, R. J. Wawak, and H. A. Scheraga, Protein Sci. **9**, 1235 (2000).
[62]S. Shimizu and H. S. Chan, J. Chem. Phys. **115**, 1414 (2001).
[63]S. Shimizu and H. S. Chan, Proteins: Struct., Funct., Bioinf. **48**, 15 (2002).
[64]L. Wang, R. A. Friesner, and B. J. Berne, Faraday Discuss. **146**, 247 (2010).
[65]S. Izvekov, J. Chem. Phys. **134**, 034104 (2011).
[66]H. W. Qi, H. R. Leverentz, and D. G. Truhlar, J. Phys. Chem. A **117**, 4486 (2013).
[67]A. S. Mahadevi and G. N. Sastry, Chem. Rev. **116**, 2775 (2016).
[68]S. N. Jamadagni, R. Godawat, and S. Garde, Annu. Rev. Chem. Biomol. Eng. **2**, 147 (2011).
[69]G. Hummer, S. Garde, A. E. García, A. Pohorille, and L. R. Pratt, Proc. Natl. Acad. Sci. U. S. A. **93**, 8951 (1996).
[70]R. Godawat, S. N. Jamadagni, and S. Garde, Proc. Natl. Acad. Sci. U. S. A. **106**, 15119 (2009).
[71]D. A. McQuarrie, *Statistical Mechanics* (University Science Books, 2000).
[72]S. Sarupria and S. Garde, Phys. Rev. Lett. **103**, 037803 (2009).
[73]M. V. Athawale, G. Goel, T. Ghosh, T. M. Truskett, and S. Garde, Proc. Natl. Acad. Sci. U. S. A. **104**, 733 (2007).
[74]S. N. Jamadagni, R. Godawat, J. S. Dordick, and S. Garde, J. Phys. Chem. B **113**, 4093 (2009).
[75]S. N. Jamadagni, R. Godawat, and S. Garde, Langmuir ACS J. Surf. Colloids **25**, 13092 (2009).
[76]H. S. Ashbaugh, S. Garde, G. Hummer, E. W. Kaler, and M. E. Paulaitis, Biophys. J. **77**, 645 (1999).
[77]I. Pagonabarraga and D. Frenkel, J. Chem. Phys. **115**, 5015 (2001).
[78]A. Chaimovich and M. S. Shell, J. Chem. Phys. **134**, 094112 (2011).
[79]S. Kullback and R. A. Leibler, Ann. Math. Stat. **22**, 79 (1951).
[80]J. F. Rudzinski and W. G. Noid, J. Chem. Phys. **135**, 214101 (2011).
[81]A. Chaimovich and M. S. Shell, Phys. Chem. Chem. Phys. **11**, 1901 (2009).
[82]M. U. Hammer, T. H. Anderson, A. Chaimovich, M. S. Shell, and J. Israelachvili, Faraday Discuss. **146**, 299 (2010).
[83]A. Chaimovich and M. S. Shell, Phys. Rev. E **88**, 052313 (2013).
[84]A. Chaimovich and M. S. Shell, Phys. Rev. E **81**, 060104 (2010).
[85]J. D. Weeks, D. Chandler, and H. C. Andersen, J. Chem. Phys. **54**, 5237 (1971).
[86]S. Plimpton, J. Comput. Phys. **117**, 1 (1995).
[87]H. J. C. Berendsen, J. R. Grigera, and T. P. Straatsma, J. Phys. Chem. **91**, 6269 (1987).
[88]J.-P. Ryckaert, G. Ciccotti, and H. J. C. Berendsen, J. Comput. Phys. **23**, 327 (1977).
[89]M. Parrinello and A. Rahman, J. Appl. Phys. **52**, 7182 (1981).
[90]C. H. Bennett, J. Comput. Phys. **22**, 245 (1976).
[91]A. Shrake and J. A. Rupley, J. Mol. Biol. **79**, 351 (1973).
[92]K. A. Sharp, A. Nicholls, R. F. Fine, and B. Honig, Science **252**, 106 (1991).
[93]L. R. Pratt and D. Chandler, J. Chem. Phys. **67**, 3683 (1977).
[94]K. Lum, D. Chandler, and J. D. Weeks, J. Phys. Chem. B **103**, 4570 (1999).
[95]F. M. Richards, Annu. Rev. Biophys. Bioeng. **6**, 151 (1977).
[96]T. Ooi, M. Oobatake, G. Némethy, and H. A. Scheraga, Proc. Natl. Acad. Sci. U. S. A. **84**, 3086 (1987).
[97]J. Kleinjung and F. Fraternali, Curr. Opin. Struct. Biol. **25**, 126 (2014).
[98]J. W. Pitera and W. F. van Gunsteren, J. Am. Chem. Soc. **123**, 3163 (2001).
[99]D. M. Huang and D. Chandler, J. Phys. Chem. B **106**, 2047 (2002).
[100]R. C. Remsing and J. D. Weeks, J. Phys. Chem. B **117**, 15479 (2013).
[101]M. E. Paulaitis, S. Garde, and H. S. Ashbaugh, Curr. Opin. Colloid Interface Sci. **1**, 376 (1996).